*Research Article*
ISSN 2304-6295
*Received: December 7, 2025* *Accepted: December 25, 2025* *Published: February 5, 2026*

# Hybrid basalt fiber aerodrome concrete performance evaluation

Qais, Qais Abdulrahman Ali[1*]
Kotlyarevskaya, Alena Valerevna[1]
Okolnikova, Galina Erikovna[1,2]

[1] RUDN University Moscow, Russian Federation; qaiseng@gmail.com ; kays_k@rudn.ru (Q.Q.A.A.); kotlyarevskaya-av@rudn.ru (K.A.V.); okolnikova_ge@mail.ru (O.G.E.)
[2] Moscow State University of Civil Engineering, Moscow, Russian Federation; okolnikova_ge@mail.ru (O.G.E.)
Correspondence:* email qaiseng@gmail.com; contact phone +79014217848

**Keywords:**

Basalt fiber; Crack; Durability; Fatigue; Fracture toughness; Fiber hybridization

**Abstract:**

Concrete airport pavements are subjected to severe mechanical and environmental demands, necessitating improved crack resistance, fatigue performance, and durability. **The object of research** is macro–micro hybrid basalt fiber reinforced concrete (BFRC) as a potential high-performance pavement material. The work aims to evaluate the influence of basalt fiber dosage and hybridization on crack width and depth, fracture toughness, fatigue life, chloride ingress resistance, and structural reliability. **Method**. Mechanical properties from laboratory tests were integrated with semi-empirical fracture mechanics models, S–N fatigue relationships, Fick's second-law chloride diffusion analysis, and reliability-based statistical assessment. **Results**. Results indicate that increasing fiber content reduced predicted crack width and depth, while hybrid systems significantly enhanced fracture parameters. The 1.5A0.5B mix exhibited the highest fracture toughness and durability performance, whereas the 2A1B mix demonstrated superior fatigue life and reliability index. Overall, balanced hybrid basalt fiber systems provided synergistic improvements in cracking resistance, fracture behavior, fatigue performance, and long-term durability for airport pavement applications.

## 1 Introduction

Concrete pavements represent the major structural elements of airport facilities. They provide for safe and efficient aircraft arrival, ground movement, and departure. The runway, taxiway, and apron slab designs need to meet the most stringent requirements for structural integrity, operational performance, and durability. These slabs must be able to resist high magnitudes of static and dynamic wheel loads and repeated landing gear impacts, surface abrasion caused by tires and rubber deposits, and exposure to fuels, de-icing chemicals, and moisture [1]. For such applications, Portland Cement Concrete (PCC) represents the basic material due to its high compressive strength, stiffness, and long-term load-carrying capability. At the same time, PCC tends to crack due to early-age and drying shrinkage, to be subjected to fatigue under repeated loading conditions, to show freeze-thaw damage, chloride penetration, and abrasion [2]. In an airport environment, these problems are exacerbated due to higher and more concentrated wheel loads, higher frequency of loading cycles, and limited opportunities for maintenance. This condition requires durability and less downtime for both operational and economic continuity [1]-[3].

These limitations are becoming increasingly urgent in view of global trends such as increased aircraft traffic, heavier single-wheel loads from new aircraft, higher expectations for pavement reliability, and the need for lower life-cycle costs. Cracking and durability failures of airfield pavements result in high operational and economic costs. Repairs are usually complex and costly, and disrupt runway availability. Growing airport demands and tighter scheduling have made these needs even more urgent, placing a

high demand for improved crack control, better fatigue performance, and greater resistance to harsh environmental conditions on concrete materials. Consequently, pavement engineering is oriented toward solutions that would not only reduce early-age cracking but also enhance post-crack toughness and load-carrying capacity, preventing the ingress of deleterious agents.

Fiber Reinforced Concrete (FRC) has emerged as a promising material class that can overcome such performance gaps. By adding discrete fibers to the cementitious matrix, FRC improves crack-bridging capacity, energy absorption, and, in general, fracture resistance. The field has evolved from early steel macrofibers to a wide range of fiber types, including synthetic fibers, such as polypropylene and polyolefins, alkali-resistant glass fibers, carbon fibers, natural fibers, and basalt fibers. A substantial body of research demonstrates that fibers improve mechanical properties, control crack development at different scales, and enhance the residual strength of concrete under repeated loading [4]-[5]. Hence, fiber inclusion has become a common strategy in pavement engineering as an effective approach towards mitigating shrinkage cracking and improving structural performance in the long run.

Among the available fiber alternatives, basalt fibers are the ones that are under focus due to their origin from naturally abundant volcanic rock, as well as showing attractive tensile and chemical stability properties; further, compared to certain synthetic alternatives, basalt fibers have favorable durability. Their unique strength, thermal stability, and environmental compatibility appear to be a promising reinforcement for high-performance pavement concretes used in aerodrome environments [6]. Basalt fibers are continuous or chopped filaments of vitreous material produced from melted basalt rock. Characteristics that may be advantageous in concrete pavements include high tensile strength, good modulus of elasticity, thermal stability, and resistance to aggressive alkali and chloride environments. Several studies reported enhancement in the Compressive and Flexuaral strength of Basalt Fiber Reinforced Concrete, as compared to plain concrete; this study also provides evidence of the importance of controlled addition of such fibers as a way to determine the optimum dosages.

### 1.1 Basalt Fiber Reinforced Concrete (BFRC)

Ashteyat et al. (2024) observed that the addition of basalt fibers had a moderate, yet consistent, enhancement in the compressive strength of BFRC up to an optimum dosage. The results of tests conducted for 0.05%, 0.10%, and 0.15% fiber contents have shown increases of 2.6%, 3.9%, and 4.4%, respectively. The maximum compressive strength of 45 MPa was achieved at a dosage of 0.15% BF, beyond which it decreased slightly to 44 MPa for a higher dosage of 0.20% BF. This implies that after reaching the optimum dosage, the positive contribution started to diminish. Ashteyat et al. believed this could be due to the fiber clustering effect and poor dispersion at higher volumes, as might result from an increase in the difficulty of mixing or loss in matrix continuity in mixtures with high fiber content. Among all these, based on test results, 0.15% was found to be the optimum dosage that balanced gain in strength with workability and dispersion of fibers.

In this regard, Hussain and Dubrey 2023 [8] tested BFRC made with higher dosages of fibers, namely 0.10%, 0.20%, and 0.30%, and found a different optimum. Indeed, their test results showed that 0.20% basalt fiber mixes gave the best compressive strength, split tensile strength, and bending strength, which were better than the lower and higher dosages tested. It therefore appears that the optimum can be expected to vary with several factors, including fiber length, surface characteristics, matrix composition, and the mixing regime applied. The conflicting findings of this work reflect the pattern observed in many recent BFRC studies: many authors report optimal performance within a narrow window of dosages. While the exact value is highly sensitive to the physical and mechanical properties of the basalt fibers tested.

In addition to dosage considerations, basalt fiber size and geometry also play significant roles in the mechanical behavior of BFRC. The most common forms of basalt fibers are available in micro- and macro-scaled forms, as shown in Figure 1 below. These micro and macro basalt fibers may either be used singly or in some combination with other fibers, referred to as hybridization, targeting various scales of cracking and mechanical response.

Macro Basalt fiber  Micro Basalt fiber

**Fig. 1 - Basalt fiber [9]**
***Image by the author of the article***

Several researchers have highlighted the advantages of hybridization of different fiber types in concrete. Hybrid methods, which combine basalt fibers with micro-synthetic or steel fibers, have shown a remarkable improvement in crack-bridging capacity, ranging from early-age microcracks due to hydration to macrocracks due to repeated aircraft gear loads. The resultant hybrid mixtures exert complementary effects; whereby mechanical functions are distributed among two or more types of fibers. These include enhanced energy absorption, improved bonding at the interface, and efficient stress transfer across the fiber-matrix interface (Gong et al., 2024 [10]; Hussain et al., 2024 [11]). This reinforcement is essential for airport pavements. Long-term structural performance is not only dependent on initial strength but also on the ability of the slab to maintain its microstructural resilience under continued operational demands.

Building on this idea, the effects of fiber length in hybrid basalt fiber systems on normal-strength (M30) and high-strength concretes (M60) were studied by Johnson et al. (2024) [12]. Here, two fiber lengths-12 mm (short) and 30 mm (long)-were used in various hybrid combinations. The total basalt fiber volume of 1.5%. The investigated mixtures included 1.5% short, 1.125% short & 0.375% long, 0.75% short & 0.75% long, 0.375% short & 1.125% long, and 1.5% long. Test results indicated that even while fiber addition reduced workability, mostly with longer 30-mm fibers due to an increase in surface area and internal friction, the compressive strength and modulus of elasticity remained rather unaffected. However, there was a significant improvement in flexural strength, especially for the HBF4 mix (1.5% total fiber volume, 25% short and 75% long), which obtained increases of 39% for M30 and 54.35% for M60. Such improvements were linked to the complementary action of short fibers in arresting microcracks and of long fibers in bridging wider cracks. Accordingly, SEM analyses showed good fiber-matrix adhesion and predominant fiber pull-out, reflecting good energy absorption and thus explaining such superior flexural performances. In all, the test outcomes identify the HBF4 hybrid configuration as the most effective by remarkably improving the flexural capacity with no loss in the other mechanical properties of the concrete, hence being very promising as a reinforcing methodology for those applications where resistance to bending and crack control is imperatively required.

In a related study, Chiadighikaobi et al. (2024) utilized two types of BF, namely Micro and Macro, to illustrate that hybridizing micro- and macro-scale basalt fibers can result in significant enhancement of compressive strength in concrete. Their best performing mix was the hybrid B4 mix, with 0.75% micro-fibers and 0.75% macro-fibers, which attained a 28-day compressive strength of 24.63 N/mm², representing a 62% improvement over the plain concrete control, B1. This enhancement was substantially higher compared to the single-fiber mixes, B2 containing 1.5% micro-fibers and B3 containing 1.5% macro-fibers. Such superior performance of the hybrid mix has been attributed to the complementary action of the two types of fibers, i.e., the bridging action as shown in Figure 2. The micro-fibers would be effective in controlling micro-cracking at early-age hydration, while the macro-fibers would bridge the larger cracks that occur under much higher applied stress levels, leading to a more cohesive and damage-resistant matrix.

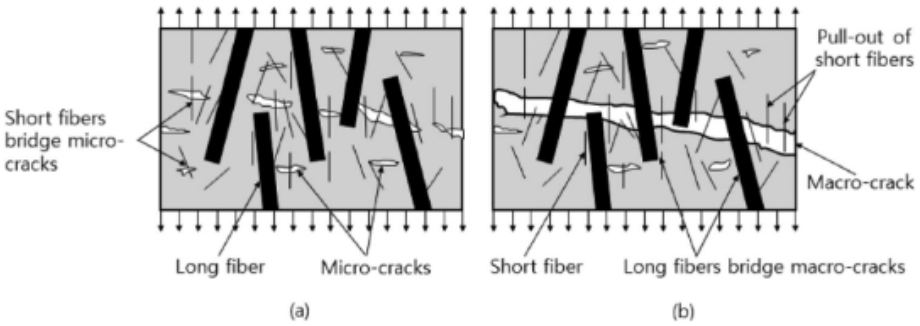


**Fig. 2 - Bridging action of the hybrid with different sizes; (a) first phase of loading, and (b) second phase of loading (Park et al., 2022 [13] as cited in Chiadighikaobi et al., 2024 [9])**
***Image by the author of the article***

Additionally, the Hybrid mix B4 also exhibited the fastest strength gain, which increased by 41% from day 7 to day 28, demonstrating that fiber hybridization acts not only to improve peak strength but also to accelerate early-age mechanical development. It is shown that hybrid fiber design plays a key role in enhancing the performance of concrete; hence, the synergism that arises from the combinations of fibers at different scales cannot be captured with single-fiber systems. This study places hybrid basalt fiber reinforcement as one of the most viable strategies toward the development of high-strength, durable, and resilient concrete for various structural and pavement applications. This observed effectiveness is partly because of crack-bridging action by the fibers, which controls crack initiation and propagation, improves post-cracking toughness, and enhances overall mechanical performance of the concrete composite.

## 1.2 Fracture mechanics.

Understanding why hybrid fibers yield such improvements requires a reconsideration of the fundamental principles that underpin crack behavior. Fracture mechanics offers a rigorous and physically grounded approach to analyzing crack initiation and propagation in concrete, which is inherently heterogeneous and quasi-brittle. The concrete microstructure, as described by aggregates, cement paste, pores, and ITZs, suggests that complex fracture behavior cannot be fully captured by the classical strength-based model. A recent review paper by Barbhuiya et al. (2024) [14] gives a broad basis on which to explore the mechanisms of crack initiation, stable and unstable crack growth, and size effects, linking microscale interactions to macroscopic fracture parameters. The synthesis highlights experimental methods for full-field deformations by means of digital image correlation and acoustic-emission techniques that detect cracking activity to characterize key fracture mechanical quantities like initiation toughness and unstable or critical toughness.

These experimental foundations have, in turn, formed the basis for substantial advances in the numerical simulation of realistic crack propagation, using various state-of-the-art numerical methods. Of these, one of the most popular for quasi-brittle materials, such as concrete, has been the phase-field model. For instance, Le et al. (2024) [15] proposed a phase-field model with an imperfect interface to model concrete at the mesoscale by explicitly accounting for aggregates, the cement matrix, and the interfaces between them. By adopting smeared scalar fields that represent cracks and interfaces, the model is capable of capturing complex fracture patterns, including debonding and bulk cracking. The strength of the interface is identified to critically influence overall fracture behavior, while this study shows that numerical simulations can be calibrated to reflect microscale physical interactions and thus provide complementary insights into experimental observations.

Apart from the static fracture behavior, another critical aspect of concrete performance is fatigue, especially when it is subjected to a sequence of loading that is repeated or cyclic in nature. In view of this, Baktheer et al. (2024) [16] have enhanced the phase-field cohesive zone method to simulate the fatigue crack propagation of quasi-brittle materials. Their model replicates experimental fatigue phenomena, including hysteresis, S–N (stress-life) curves, fatigue creep, and Paris-law behavior. This work demonstrates that accurate modeling of fatigue is now possible and provides a predictive tool for the long-term structural performance of concrete, a subject area for which fracture mechanics has traditionally struggled to find solutions by validating the approach across two- and three-dimensional boundary-value problems and different crack modes, mode I, and mixed-mode.

Other numerical frameworks have also emerged. Alrayes et al. (2023) [17] applied the scaled boundary finite element method (SBFEM) coupled with a cumulative damage-plasticity constitutive law to simulate cyclic crack growth. The approach they propose allows for detailed modeling of the FPZ due to the consideration of cohesive traction laws that were corrected for damage accumulation during load cycles and has been able to capture the monotonic and fatigue-driven crack growth in heterogeneous concrete under load. These complementary modeling strategies illustrate the increasingly sophisticated and accurate fracture mechanics tools.

Experimental investigations have continued to provide vital validation to such models. As an example, Wei Dong (2024) [18] explored the quasi-static and dynamic fracture behavior of mass concrete, with special attention to large-scale members under extreme loading, such as those experienced by dam structures. Employing pre-cracked cylindrical specimens under different loading rates, the investigation showed well-pronounced differences in the fracture response between the quasi-static and dynamic conditions, thus yielding practical information on fracture energy, crack growth, and size effects in field-relevant situations.

The principles of fracture mechanics are particularly useful in the design of fiber-reinforced or modified concretes. Recently, research involving basalt fiber-reinforced expanded-polystyrene geopolymer concrete has demonstrated how effective fiber bridging is at improving fracture properties. In the investigation of Tao et al. (2025) [19], critical parameters of fracture, such as initial fracture toughness, unstable toughness, fracture energy, and ductility index, were determined by notched beam three-point bending and DIC. These authors demonstrated some impressive gains for these properties, including a 98.9% gain in fracture energy and a greater than 28% gain in unstable toughness, which was primarily due to the energy-dissipating, crack-bridging action of the fibers, as confirmed through microscopy and X-ray micro-CT analyses.

Hybrid fiber systems, which combine fibers of different lengths or types, are increasingly being examined through a fracture-mechanics lens. Ding et al. (2025) [20] studied hybrid fiber-reinforced concrete (HFRC) combining basalt fibers (BF) and polypropylene fibers (PPF). Static and dynamic mechanical tests, in concert with microstructural characterization, demonstrated a synergistic effect at an optimal BF-to-PPF ratio of 1:2 by volume: the compressive strength was enhanced by 13.7%, the splitting tensile strength by 76.3%, and the elastic modulus by 116%. These microstructural observations have demonstrated that, indeed, fibers effectively bridge cracks, distribute stress, and resist pull-out, leading to enhanced toughness and energy absorption.

These various studies together give evidence of the merging of experimental, theoretical, and computational efforts in fracture mechanics to understand and improve concrete performance. They have shown that current modeling techniques allow the engineering of stronger, more damage-tolerant, and durable concretes under realistic loading and environmental conditions when combined with fiber-reinforced approaches. Based on this body of work, Khan et al. (2021) [21] further investigated the effects of basalt fiber length and dosage on fracture behavior, reinforcing the key role of fiber geometry in tailoring mechanical performance.

### 1.3 Crack Behaviour of FRC

Cracking in concrete represents the fundamental challenge to pavement durability, especially for rigid airfield pavements where restrained shrinkage, thermal gradients, and drying shrinkage interact to cause microcrack formation that can grow into full-depth cracks. Key to FRC's enhanced resistance to crack formation is the fiber-bridging process. When concrete cracks, the fibers crossing the crack carry tensile stresses, restrain crack opening, retard propagation, and dissipate energy. Consequently, there is an increase in the energy involved in crack initiation and growth, thereby enhancing toughness and residual load capacity. Theoretical underpinnings for this behavior were given by fracture-process-zone models, such as the cohesive (fictitious) crack model, representing a nonlinear zone of microcracking and bridging near the tip of the crack that governs post-cracking response Zhang et al. (2024) [22].

Building on this concept, Khan et al. (2021) [21] have quantified the influence of basalt fiber geometry through tests carried out on mixes containing four kinds of fiber lengths, namely, 12, 25, 37, and 50 mm. In fact, the FCSF-BF12c composite containing 0.45% of 12 mm basalt fibers performed better than all other mixes in terms of both the initial fracture toughness and fracture energy. This enhancement was explained with respect to optimum fiber bridging that restricted the development of meso-cracks and macro-cracks during both stable and unstable crack propagation modes. SEM observations also confirmed that energy-absorbing mechanisms such as fiber pull-out, breakage, and adequate bonding played an important role in improving fracture resistance. The above studies

demonstrate the importance of fiber length and content optimization towards a balanced and efficient crack-control system in FRC.

Complementing this work, da Silva et al. (2025) [23] have emphasized the importance of the fiber–matrix interfacial behavior in controlling crack development. Thus, depending on whether pull-out, debonding, or breakage is the mode of fiber failure, energy dissipation will take place accordingly during cracking. For example, in the case of pull-out, the energy will be dissipated through friction and debonding processes. In agreement with Khan et al. (2021), Da Silva et al. have established that the employment of shorter fibers provided a more positive contribution to fracture toughness due to the enhancement of the bridging mechanism and limitation of microcrack opening. Their findings also suggest improvements in the compressive and flexural strength usually accompanying enhancements in fracture toughness.

Beyond interfacial and bridging mechanisms, the flexural performance of hybrid fiber systems has been widely explored. One such work is by Fu et al. (2022) [24], where it is observed that the combined use of basalt and polypropylene fibers at low volume fractions resulted in increased ductility with modified fracture paths along with improved residual strength. The tortuousness introduced in the crack path by the multiple fiber types reduced the possibility of straight, catastrophic crack growth. This behavior is of particular interest for airfield pavements, since concentrated aircraft wheel loads may propagate cracks rapidly unless effectively resisted by fiber reinforcement.

Further supporting the benefits of fiber addition, a study by Zhang et al. (2025) [25] demonstrated that with increased volume of steel fibers, compressive strength, fracture toughness, and fracture energy were enhanced. More specifically, with the increase in the volume of steel fibers by 21%, enhancements of 45.45% and 2013.4% were recorded with regard to fracture parameters when compared to the control mix. These observations led the authors to conclude that the incorporation of fibers for maximum improvement in fracture toughness and fracture energy should be done in a controlled manner.

The environmental durability has also been explored. Pei et al. (2024) [26] conducted Split-Hopkinson Pressure Bar testing on BFRC to investigate dynamic fracture performance after exposure to freeze-thaw cycles. They reported that an increase in FTC exposure promotes crack growth and decreases dynamic Mode I fracture toughness. Of importance, longer basalt fibers oriented perpendicular to the crack tip were found to decrease Mode I stress intensity factors more effectively than Mode II, again highlighting how fiber geometry and orientation influence dynamic fracture resistance under cyclic freeze-thaw conditions.

Similarly, Tao et al. (2025) [27] explored the properties of basalt fiber-reinforced EPS-geopolymer concrete. Notched three-point bending and digital image correlation provided significant improvements in various fracture parameters at the respective optimums of 0.4% fiber and 20% EPS, including 99% improvement in fracture energy and ~28% gain in unstable toughness. Microscopy and X-ray micro-CT imaging confirmed that fiber bridging, pull-out, and crack deflection dominated the toughening response.

Overall, the evidence from the studies indicates that there is a direct proportional relation between fracture parameters related to fiber-reinforced concrete and the resulting crack width and depth, with implications for fiber design in controlling cracking and improving structural performance. Saouma (2022) [28] Fracture mechanics notes indicated that $K_{1c}$. is dependent on the crack depth as shown in Equation 1. This shows that the $K_{1c}$ is directly proportional to crack depth ( $d$ . ) i.e., a greater $d$ would result in a greater $K_{1c}$. In addition, proving that a greater Crack width ( $w$ ) would also result in a greater $K_{1c}$. This is because the $w$ is also directly proportional to the $d$ as shown in Equation 2.

$$K_{1c} = Y\sigma\sqrt{(\pi d)}, \quad (1)$$

[28]

where $Y$ is the geometry Factor and $\sigma$ is the applied far-field tensile stress.

$$d = kw. \quad (2)$$

[29]

## 1.4 Fatigue Life of FRC

Fatigue behavior in pavement concrete differs considerably from the classic fatigue phenomena observed in conventional structural members. While beams or columns usually experience distributed stresses over larger areas, pavement slabs are exposed to highly concentrated contact stresses due to aircraft wheels. The magnitudes of the loads are much higher, while the areas of loading are relatively

small, and the number of load repetitions on intensively used runways can reach hundreds of thousands to several millions during the pavement service period. Thus, mechanisms of fatigue crack initiation and propagation in pavement concrete are controlled not only by the magnitude and frequency of traffic loads but also by a complex interaction among static and dynamic wheel pressures, subgrade stiffness, joint conditions, temperature gradients, and long-term environmental deterioration processes such as moisture ingress or freeze-thaw cycles. This multi-factor nature of pavement fatigue demands a rigorous understanding of the different methodological approaches used in its assessment.

Various established methods for testing the fatigue performance of concrete pavement specimens generally fall into experimental, numerical, and empirical categories. Experimental approaches include flexural fatigue testing, direct tensile fatigue testing, accelerated pavement loading, fracture-based cyclic testing, and full-scale pavement simulators. These remain some of the most physically representative techniques for characterizing how cracks initiate, interact, and propagate under repeated stresses [30]-[31]. Investigation of material heterogeneity, fiber-matrix bonding characteristics, microstructural defects, moisture effects, and realistic modes of failure should be feasible with such studies, both in the laboratory and the field, which purely theoretical or computational models can seldom reproduce with high fidelity. Despite accuracy and realism, these experimental procedures are usually time-consuming, highly equipment-dependent, and costly; for these reasons, they are less viable for routine design applications or large-scale assessments.

At the same time, empirical methods are a more practical alternative in those cases when rapid assessment or interpretation of extensive datasets is required. Several techniques widely used in practice for preliminary pavement designs or to assess fatigue life in pavement management systems include S-N relationships of fatigue, the Miner's cumulative damage hypothesis, and regression-based models of fatigue prediction obtained from historic pavement performance databases [32]-[33]. These methods simplify the complex fatigue behavior of concrete into tractable mathematical expressions, whereby engineers can approximate performance without extensive testing. These models lack the depth and mechanistic accuracy of experimental studies but have been effective at capturing broad trends in fatigue and for decision-making in large infrastructure networks. It is in the balance between simplicity and predictive capability that empirical models become indispensable under certain conditions when resources, time, or equipment availability is lacking.

A growing body of research also underlines the influential role that fibers can play in enhancing fatigue crack resistance and lengthening service life in asphalt and concrete pavements. The fact that fiber reinforcement constrains microcrack formation and ultimately suppresses the generation of macrocracks, as well as improving load transfer across developing fracture planes, has been clearly demonstrated. However, performance improvements brought about by the application of fibers are very often quite variable with respect to fiber type, geometry, aspect ratio, surface texture, and dosage. Qin et al. (2024) [34] pointed out that adding steel fibers significantly improved the mechanical properties of concrete, including those related to its fatigue performance, mainly because such fibers improve post-cracking behavior and fracture toughness. This, of course, further reinforces the general principle that increased fracture toughness is directly proportional to improved fatigue resistance, given that tougher materials dissipate more energy during crack growth and hence result in slower fatigue degradation.

In this regard, hybrid fiber reinforcement approaches have received greater attention in recent times. Hybrid systems comprise micro-fibers like polypropylene, basalt micro-fibers, or cellulose fibers, combined with macro-fibers such as steel, basalt, and other synthetic macro reinforcements. The idea is to exploit each of the strengths of these fiber types: while micro-fibers are highly effective in controlling plastic shrinkage and limiting early microcrack development, macro-fibers contribute to post-cracking load transfer and structural bridging at larger crack widths. Singh et al. (2012) [35] showed that hybrid fiber concrete had lower crack propagation rates compared to unreinforced and single fiber concrete mixtures and resists a greater number of load cycles to failure. Besides improving fatigue, hybridization has also been attributed to broader improvements in durability performance, including resistance to impact, abrasion, spalling, and environmental degradation. Multiple fiber types combined provide a synergistic reinforcement mechanism capable of dealing with a wide range of modes of failure in pavement systems and enable longevity with reduced maintenance needs.

## 1.5 Durability of BF Pavement

Durability testing of BF pavements has to link material-scale transport and chemical degradation processes with the pavement-scale mechanical wearing and environmental cycling [36]. Experimental durability tests of BF concrete commonly address only the permeability and transport properties, such as water absorption, sorptivity, rapid chloride migration, or RCPT, etc. Besides freeze-thaw resistance, salt

scaling, and combined salt-freeze tests, abrasion and skid resistance, and microstructural tests also play an important role in determining the durability of reinforced pavement [37-38]. Standardised, accelerated tests, such as non-steady state chloride migration and ASTM C666 freeze-thaw and abrasion tests, are in extensive use because they compress the long-term processes into the laboratory timeframe yet can still reveal the comparative behaviour across the mixes [37]. Testing is necessary, since the effects of BF are often indirect. fibers change the cracking patterns, tortuosity, and microcrack bridging that, in turn, affect transport and surface deterioration more than they directly change the bulk chemistry.

When properly dosed and dispersed, basalt fibers have shown a net positive effect in several durability metrics in recent laboratory and field studies. These include reports of reduced surface scaling under salt-freeze cycles and improved retention of dynamic modulus in freeze-thaw testing owing to crack-control effects. That is, smaller and better-distributed microcracks, enhanced post-crack bridging, and pore connectivity alterations yield slower ingress. For example, Zhou et al. (2023) [39] determined that small basalt-fiber additions improved mortar resistance to salt-freeze erosion and significantly limited mass loss by preserving the pore structure and minimal macrocrack development. Similar improvements in frost resistance and reduced permeability for BF-modified concretes have been reported by Guo et al.(2024) [38] from their experimental study. These are consistent with a premise that the principal durability benefit of BF in pavements is crack control and the associated reduction of pathways for aggressive agents, rather than large gains in intrinsic chemical resistance.

However, gains in terms of durability are also strongly dependent on fiber content, length, dispersion, matrix composition, and fiber surface treatment. Several works observe an optimum dosage of BF beyond which workability and clumping of fibers impair consolidation, increasing entrapped air, and creating zones of weakness that can further worsen permeability and surface wear [36], [12]. Besides that, the interface between BF and cementitious matrix-the ITZ-is a critical issue. If some sizing or surface modifications are not used, eventually, an untreated BF could be susceptible to alkaline attack or poor bonding with high-alkalinity cement matrices for very long exposure. Wang et al. 2025 [40] pointed out that modified or nano-treated basalt fibers-silane/nano-$SiO_2$ coating to improve chemical stability and adhesion. First test results show improved durability metrics compared to unmodified fibers. Thus, mix design and fiber treatment will become the effective prerequisites for assuring that BF's theoretical advantages are realized in the reliable performance of pavement.

The key weaknesses and degradation pathways of BF in pavement contexts are still under investigation. Some of the more fundamental issues include long-term chemical stability of basalt fibers in highly alkaline pore solutions, possible mineral leaching from the fibers, and how repeated mechanical polishing/abrasion may affect the surface-exposed fibers. Such uncertainties underline the fact that, while basalt fibers have demonstrated distinct advantages in controlled conditions, their complete performance over a long period when placed under natural pavement conditions is not yet fully known.

Despite undisputed evidence from the laboratory of basalt fibers and hybrid fiber approaches for mitigating cracking and enhancing toughness, what still appears to be lacking is holistic, integrated performance evaluations presenting quantitative measures for cracking behavior, fatigue life under representative pavement loading, and durability under environmental stressors for basalt fiber hybrid pavement mixes. This research, therefore, tries to fill such a gap by developing and applying an integrated multi-criteria performance-evaluation methodology for basalt fiber hybrid concrete pavements. The goal is to evaluate and rank pavement mix alternatives (Plain concrete, Basalt-fiber-Only, and Basalt–Hybrid fiber mixes) with respect to a combined set of technical parameters, namely crack width and density, fatigue life, and chloride ingress. Therefore, the objective in this study is as follows:

1. To investigate the crack width, depth, and propagation of hybrid macro-micro basalt fiber reinforced pavement concrete through semi-empirical analytical models and using experimentally determined mechanical properties.
2. Fracture performance, namely fracture toughness and energy release rate of each BFRC mix, and the role of fiber hybridization in resisting brittle failure.
3. To evaluate the durability and fatigue performance of BFRC pavement mixes by estimating chloride ingress, deterioration rate, and fatigue life through established analytical approaches and S–N modeling.
4. To perform a statistical reliability analysis to quantify the expected number of cracks and structural reliability of each BFRC mix and identify the optimal hybrid fiber combination for pavement applications.

# 2 Materials and Methods

This chapter outlines the methods adopted for characterising the cracking behaviour, fracture characteristics, fatigue performance, durability, and structural reliability of the laboratory-tested macro-micro hybrid basalt fiber-reinforced concrete pavement samples. A section on integrated experimental, analytical, and semi-empirical modeling is presented. According to this approach, the methodology followed four key steps. First, mechanical properties were extracted from laboratory tests and finite element (FE) analysis. Second, crack width, crack depth, fracture toughness, fatigue life, and chloride-diffusion-based deterioration parameters were derived using appropriate and validated semi-empirical models. Third, the expected occurrence of cracking was estimated using statistical and reliability-based methods. Finally, a comparative performance assessment was conducted for all concrete mixes.

All the equations and procedures for modeling in this analysis were based on the existing design frameworks for fiber-reinforced concrete and fracture mechanics models that have been rigorously supported by recent studies.

## 2.1 Concrete Mechanical Properties

25 concrete mixes were analyzed in this study. The used Mechanical properties i.e Compressive strength and Flexural strength, are as in Table 1.

**Table 1: Concrete Specimens**

| S/n | Percentage of Basalt Micro fiber (A) | Percentage of Basalt Macro fiber (B) | Name | Compressive Strength(MPa) | | | Modulus Of Elasticity (GPa) | 28-Day samples Flexural Strength (MPa) |
|---|---|---|---|---|---|---|---|---|
| | | | | 7-Day | 14-Day | 28-Day | | |
| 1 | 0 | 0 | K | 51.67 | 58.33 | 63.6 | 51.5 | 8.8 |
| 2 | 2 | 0 | 2A | 47.45 | 52.8 | 58.4 | 50.4 | 9.5 |
| 3 | 1.5 | 0 | 1.5A | 50.18 | 54.36 | 60.76 | 51.96 | 9.9 |
| 4 | 1 | 0 | 1A | 54.9 | 62.5 | 70.86 | 53.57 | 9.3 |
| 5 | 0.5 | 0 | 0.5A | 53.152 | 60.5 | 67.7 | 50.98 | 8.9 |
| 6 | 0.25 | 0 | 0.25A | 49.4 | 53.5 | 60.5 | 49.3 | 8.6 |
| 7 | 0 | 2 | 2B | 51.53 | 57.55 | 66.67 | 51.7 | 9.2 |
| 8 | 0 | 1.5 | 1.5B | 49.9 | 56.37 | 63.03 | 51.85 | 9.5 |
| 9 | 0 | 1 | 1B | 52.72 | 58.42 | 68.5 | 52.73 | 9.7 |
| 10 | 0 | 0.5 | 0.5B | 46.66 | 52.71 | 58.67 | 50.3 | 9.3 |

| | | | | | | | | |
|---|---|---|---|---|---|---|---|---|
| 11 | 2 | 1 | 2A1B | 52.7 | 57.5 | 64.15 | 52.7 | 9.4 |
| 12 | 2 | 0.5 | 2A0.5B | 48.6 | 52.3 | 58.8 | 51.8 | 9.6 |
| 13 | 1.5 | 2 | 1.5A2B | 48.4 | 53.8 | 59.28 | 52.2 | 9.7 |
| 14 | 1.5 | 1.5 | 1.5A1.5B | 51.3 | 57.63 | 63.87 | 53.3 | 10.2 |
| 15 | 1.5 | 1 | 1.5A1B | 52.1 | 57.04 | 63.74 | 52.97 | 9.5 |
| 16 | 1.5 | 0.5 | 1.5A0.5B | 56.8 | 63.87 | 72.8 | 53.65 | 10.4 |
| 17 | 1.5 | 0.25 | 1.5A0.25B | 52.8 | 59.18 | 67.13 | 52.4 | 9.4 |
| 18 | 1 | 2 | 1A2B | 53.96 | 59.76 | 67.46 | 52.13 | 10.1 |
| 19 | 1 | 1.5 | 1A1.5B | 49.34 | 54.65 | 60.2 | 52.7 | 10.3 |
| 20 | 1 | 1 | 1A1B | 51.52 | 58.4 | 66.156 | 51.3 | 9.7 |
| 21 | 1 | 0.5 | 1A0.5B | 49.34 | 57.3 | 63.71 | 51.05 | 9.4 |
| 22 | 0.5 | 2 | 0.5A2B | 51.34 | 56.99 | 64.8 | 51.3 | 9.4 |
| 23 | 0.5 | 1.5 | 0.5A1.5B | 52.23 | 57.4 | 64.42 | 51.92 | 9.9 |
| 24 | 0.5 | 1 | 0.5A1B | 50.6 | 56.5 | 65.47 | 51.37 | 9.5 |
| 25 | 0.5 | 0.5 | 0.5A0.5B | 49.813 | 54.2 | 62.02 | 50.52 | 9.1 |

The compressive and Flexural strength of samples were obtained from previously conducted compressive strength tests, as shown in Figure 3-4 and Equation 3-4 for the 7, 14, and 28-day samples. The Modulus Elasticity was then derived using Equation 5

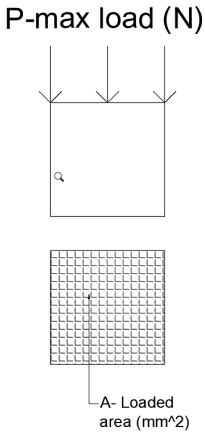


**Fig. 3 - Compressive strength cube test**
***Image by the author of the article***

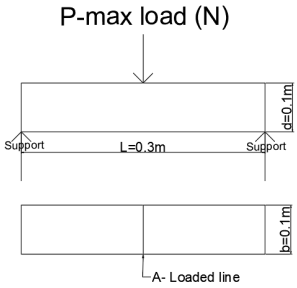


**Fig.4 - Three-point loading flexural strength test of a beam**
***Image by the author of the article***

$$f_C = \frac{\text{Maximum Load}}{\text{Cross sectional area of the sample}}, \quad (3)$$

$$f_r = \frac{3PL}{2bd^2}, \quad (4)$$

where P is the maximum load; L is the length; b is the width of the sample; d is the depth of the sample

$$E_e = \frac{\sigma_2 - \sigma_1}{e_2 - e_1}, \quad (5)$$

where;

$\sigma_1, \sigma_2$ = stress values within linear portion of stress–strain curve (MPa)

$e_1$, $e_2$ = corresponding strain values

## 2.2 Crack Width and Depth Analysis

The crack width was derived from the Mean crack spacing ($S_m$), Strain reduction factor ($\beta$), and tensile strain at the fiber level ($\varepsilon_s$) as shown in Equation 6 [1].

$$W = S_m \cdot \beta \cdot \varepsilon_s, \quad (6)$$
[41]

The Strain reduction factor ($\beta$) is a dimensionless coefficient that shows how much tension the concrete and fibers still carry between cracks. It adjusts for the difference between the strain at a crack and the average strain in the concrete. $\beta$ typical values range from 0.4 to 1.0; the $\beta$ value used for the

control mix (no fibers) was 0.6. While a constant $\beta$ value used for the rest of the fiber mixes was 0.8. At 28 days, all fiber mixes' compressive strength was greater than the control mix; thus, the greater the $\beta$ value used [42].

The $S_m$ value used for the control mix was 0.15m because the cracks observed from the experimental test were much closer than plain reinforced concrete. This estimation aligns with Vandewalle's (2023) [43] study. While the $S_m$ value used low fiber content (A+B<1.5%) was 0.12m and 0.10m for large fiber content (A+B$\geq$1.5%). The $S_m$ values are dependent on reinforcement spacing, bond characteristic, and fiber content. Smaller $S_m$ means more frequent but finer cracks, hence validating the values used.

The $\varepsilon_s$ value of mixes was dependent on several values i.e. tension stress ($\sigma_s$), Flexural strength (modulus of rupture) ($f_r$), compressive strength($f_c$), Modulus of elasticity ($E_c$ ). (See Equations 7-9).

$$f_r = 0.7\sqrt{f_c}, \quad (7)$$ [41]

$$\sigma_s = 0.3 f_r, \quad (8)$$ [41]

$$\varepsilon_s = \frac{\sigma_s}{E_c}, \quad (9)$$ [41]

The Compressive strength values were used from previously conducted compressive tests (see Table 1). The modulus of rupture of 28-day used was also obtained from a previously conducted 3-point loading test (see Table 1). While the 7-day and 14-day were estimated using Equation 7. After deriving the Crack width, the Crack depth was determined using Equation 2 [29]. Under service and shrinkage loads, several works find a linear depth-width scaling for small cracks, i.e., cracks<0.3mm. Zhu et al. (2020) [29] study shows near linear scaling; thus, this study adopted a pragmatic linear scaling constant.

## 2.3 Crack Propagation Analysis

The critical fracture toughness ($K_{1c}$. ) is the value of $K_1$ at which unstable crack growth starts. It is a fundamental parameter in fracture mechanics that quantifies the magnitude of the stress field near the tip of a sharp crack in a linear-elastic material. As shown in Equation 10, this value is dependent on several parameters, such as the maximum load (in Newtons, N) recorded during the three-point bend test ($P_m$) (see Figure 4), and the total weight of the beam between the supports (in kg). The term $0.5Wg$ accounts for the contribution of the specimen's self-weight to the bending moment, Acceleration due to gravity($g$) (9.81 m/s²), the span length of the beam between the supports ($S$), the notch depth ($\alpha$), the width of the beam ($b$), and the depth of the beam ($d$).

$$K_{1c}\ (\mathrm{MPa}\sqrt{\mathrm{m}}) = 3(P + 0.5Wg)\frac{S\sqrt{\alpha}}{2bd^{3/2}} f(\alpha), \quad (10)$$ [44]

$$\text{where } f(\alpha) = \frac{1.99 - \alpha(1-\alpha)(2.15 - 3.93\alpha + 2.7\alpha^2)}{\sqrt{\pi}(1+2\alpha)(1-\alpha)^{3/2}}.$$

The Energy release rate ($G$), on the other hand, tells how much potential energy is released per unit increase in crack area. The derived Energy release rate was dependent on the critical fracture toughness ($K_1$), Modulus of Elasticity ($E$), and Poisson's ratio (v) as shown in Equation 11.

$$G = \frac{K_I^2}{E'} \quad \text{where } E' = \begin{cases} E \text{ (plane stress)} \\ \dfrac{E}{1-V^2} \text{ (plane strain)} \end{cases}, \quad (11)$$ [44]

## 2.4 Durability Analysis

Durability properties of samples were determined from the deterioration rate and Fatigue life. Fick's 2nd-Law analytical solution for chloride ingress was used to estimate the Deterioration rate of the samples. A closed-form solution for time to reach a given threshold chloride concentration at cover depth (x) was adopted as shown Equation 12

$$t = \frac{[\mathrm{erf}^{-1}(1-\frac{C_{th}}{C_s})]^2 \ x^2}{D_{app}}, \quad (12)$$ [45]

Surface chloride concentration ($C_s$) was assumed to be 0.6 (wt% cement), which is typical of splash/marine exposure [46]-[47]. While the threshold chloride ($C_{th}$) value used was 0.4 (wt% cement), a conservative value which also aligns with many studies [46]. The cover depth (x) used was 50mm. The Baseline apparent diffusion ($D_{app}$) value used was dependent on the derived compressive strength, with several studies reporting that higher denser and compressive strength mixes resulted in a lower diffusion. In accordance with this, a commonly applied empirical scaling was used as shown in Equation 13.

$$D \propto f_c^{-0.5}, \quad (13)$$ [45]

The Fatigue life was estimated using the stress–life (S–N) approach as the most feasible and widely accepted method for basalt fiber-reinforced concrete (BFRC) mixes. In this method, a logarithmic S–N relationship between the cyclic stress level and the number of cycles to failure was established, using the ratio of applied stress to static flexural strength as the governing parameter. This approach has been extensively applied in recent BFRC studies, which demonstrated that the inclusion of basalt fibers enhances fatigue resistance, particularly at optimal fiber contents of around 0.3%. The fatigue behavior was dependent on several parameters, as shown in Equation 14.

$$\log_{10}N = \alpha + b \log_{10}(S_{rel}) \ \text{ where } S_{rel} = \frac{\sigma_{Cyclic}}{f_r}, \quad (14)$$ [48]

Here, $N$ demotes the number of cycles to failure, $\sigma_{Cyclic}$ represents the cyclic stress amplitude, which was derived from Von-Mises stress results, hence it was mix dependent. The fatigue strength coefficient ($\alpha$) used was 4.8908, while the fatigue strength exponent (b) used was -5.0. Typical $b$ can range from -3 to -7 for fiber-reinforced concrete [48-49].

## 2.5 Statistical Analysis

The Statistical analysis results were also derived from a commonly used semi-empirical approach. A combined statistical and reliability-based analysis to evaluate crack occurrence and performance reliability of macro-/micro-basalt fiber reinforced concrete (BFRC) pavement models. The deformation results were obtained from the FEA, i.e., 28-day maximum static deformation under aircraft wheel contact, and were incorporated in Equation 15.

$$D_i \sim N\mu_{i,}\sigma_i = COV * \mu_{i,}, \quad (15)$$ [50]

Where each deformation value ($D_i$) was treated as the mean ($\mu_i$) of a random variable $D_i$ representing the potential deformation of the pavement slab. In the absence of direct experimental standard deviations, a coefficient of variation (COV) of 2 % was assumed to capture material and model uncertainties. A serviceability threshold deformation, $d_{crit} = 0.00585 \text{ mm},$ . was also adopted to represent the onset of surface cracking, and the probability of crack occurrence (failure probability) for each mix was determined (see Equation 16).

$$P_{f,i} = P(D_i > d_{crit}) = 1 - \phi\left(\frac{d_{crit} - \mu_{i,}}{\sigma_i}\right), \quad (16)$$ [50]

Where $\phi$ is the standard normal cumulative distribution function. An expected-crack proxy was then used to estimate by scaling a baseline poison intensity, i.e., two cracks per slab for the control mix, as shown in Equation 17.

$$\lambda_i = 2 * \frac{P_{f,i}}{P_{f,control.}}, \quad (17)$$ [50]

After the failure probability ( $P_{f,i}$ ) value was obtained, it was then input into Equation 18 to determine the reliability index for each mix. Hence, lower $P_f$ values resulted in higher $\beta_i$ , indicating improved resistance to cracking.

$$\beta_i = -\phi^{-1}(P_{f,i}, \quad (18)$$ [50]

# 3 Results and Discussion

## 3.1 Crack Width and Depth Results

The derived $W$ for 7-day and 14-day samples indicate that the 0.5A sample is expected to have the greatest crack width regardless of the day of the sample. While the derived $W$ for 28-day shows that 1B possessed the highest Crack width. On the other hand, the Min crack results were not constant. The 1.5A2B (7-day) sample possessed the minimum crack width for 7-day samples with a crack width of 0.00224mm (See Figure 5), while the 2A0.5B (14-day) sample possessed the minimum crack width for 14-day samples with a crack width of 0.00235mm (See Figure 5). The 1A1.5B (28-day) sample possessed the minimum crack width for 28-day samples with a crack width of 0.00247mm (See Figure 5). From the derived results, it was observed that the samples with higher fiber content possessed the least crack width, thus concluding that an increase in the fiber content would result in a decrease in expected crack width. These results align with several other studies; for example, Xue et al.(2023) [51] noted that the importance of early-age hydration and bond development can lead to improved crack resistance, hence reducing the crack width of concrete. In a related study, Anas et al (2022) [52] noted that an increase in fiber ratios would result in main crack widths, increase post-crack toughness, and produce closely spaced, tighter cracks

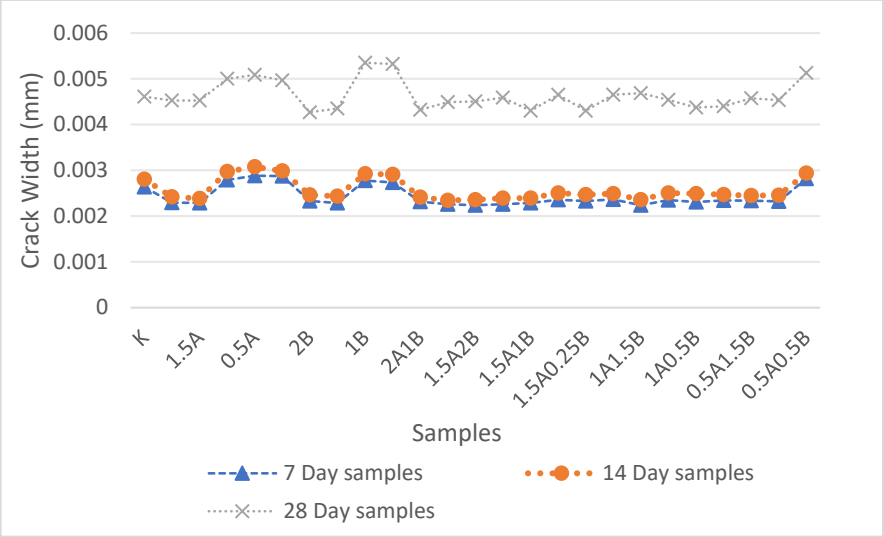


**Fig. 5 - Crack width of samples**
***Image by the author of the article***

The $d$ was directly proportional to crack width results, thus the 0.5A sample possessed the greatest crack depth regardless of the day of the sample (see Figure 6), i.e., 7, 14, and 28 days. Moreover, the same conclusion was reached that the samples with greater fiber content possessed the least crack depth, thus also suggesting that an increase in fiber content would result in reduced crack

depth. These results also align with Anas et al (2022) [52], stating increase in fiber ratios would improve the cracking resistance of concrete, hence reducing the crack depth.

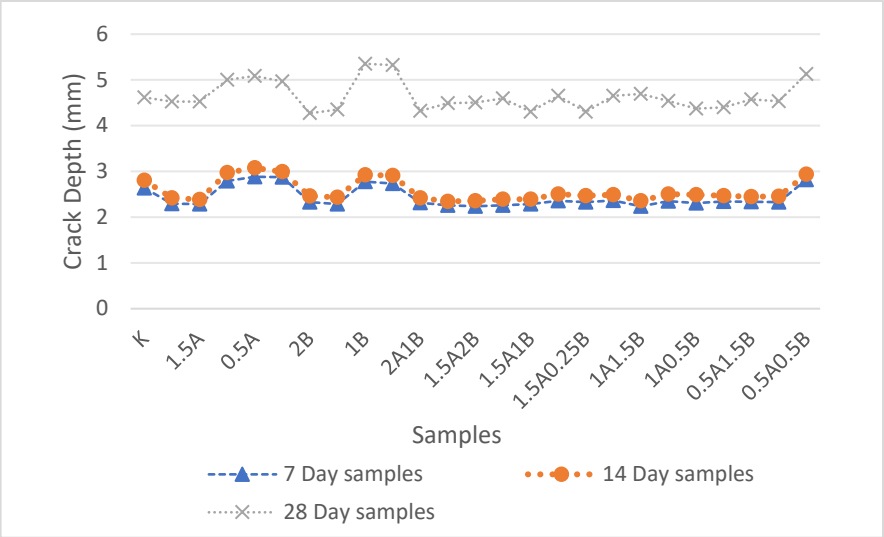


**Fig. 6 - Crack depth of 7-day samples**
***Image by the author of the article***

## 3.2 Crack Propagation Results

The derived $K_{1c}$ values show 28-day samples possessed higher $K_{1c}$ values (See Figure 7), due to higher compressive and flexural strength to resist higher loads. In addition, it was observed that the 1.5A0.5B sample for 7, 14, and 28 days. Sample possessed the highest $K_{1c}$ values among their counterparts (see Figure 7). Thus, suggesting the 1.5A0.5B sample was the least brittle material. These results also align with Chiadighikaobi et al. (2022) [53] study, which indicated that an increase in fiber ratios would reduce the brittleness, hence increasing the fractural toughness of the concrete.

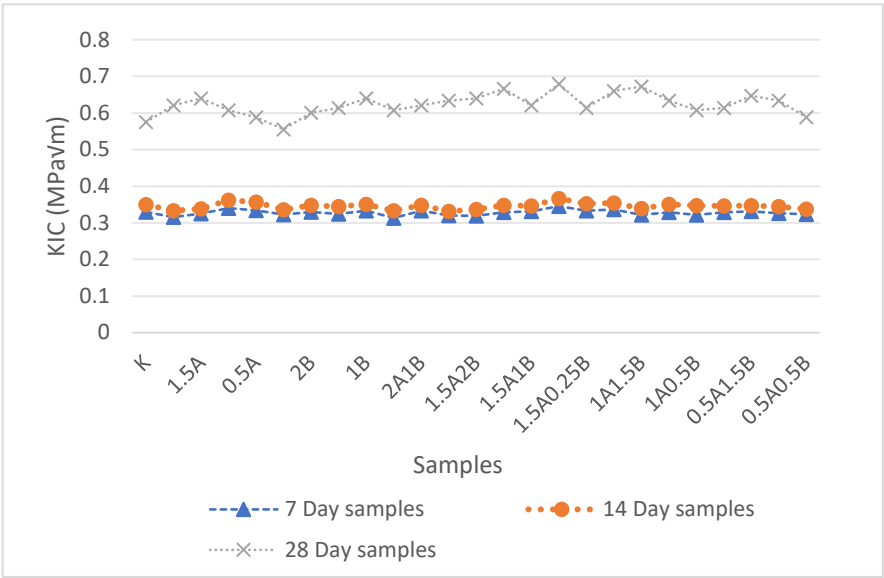


**Fig. 7 - Derived $K_{1c}$ values of samples**
***Image by the author of the article***

The derived $G$ values also showed improvement in the 1.5A0.5B sample across the 7-, 14-, and 28-day sample counterparts (see Figure 8). A significant derivation of result was also observed in 2A and 1.5A samples across the 7-, 14-, and 28-day samples, thus suggesting the elastic modulus of concrete samples have great influence on the $G$ value of the sample than the $K_1$. These results also align with Chiadighikaobi et al. (2022) [53] study, which concluded that an increase in the fiber content and reduced

Poisson ratio would result in reduced crack generation of the concrete, thus increasing the Energy release rate.

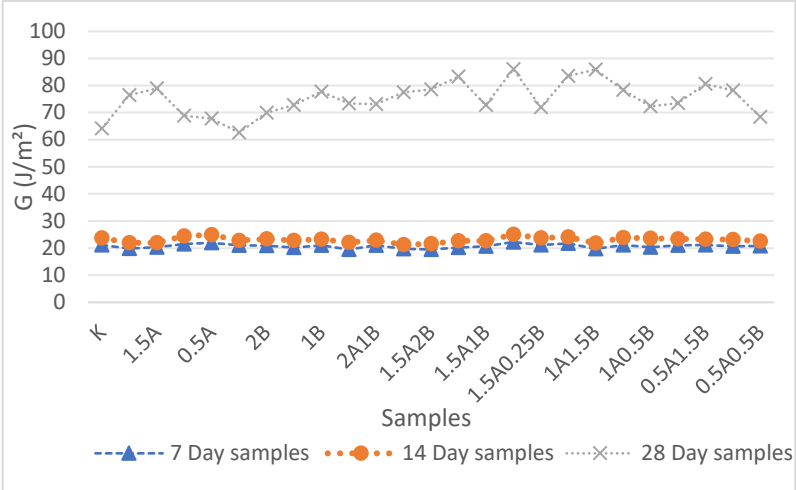


**Fig. 8 - Derived G values of the samples**
***Image by the author of the article***

## 3.3 Durability Results

The values of derived deterioration values show that 1.5A0. 5B is the most durable concrete and might potentially have the highest matrix strength to resist chemical attack over time. This performance is directly related to the higher compressive strength, due to which the chloride diffusion rate is low. Results confirm that modification in mix design, in particular reduction of component B, significantly enhances durability and prolongs the service life of the structure in comparison with the standard baseline mix (see Figure 9). These results also align with Razmi et al. (2025) [54] study which noted that mixes with higher 28-day compressive strengths generally have lower measured chloride diffusivity.

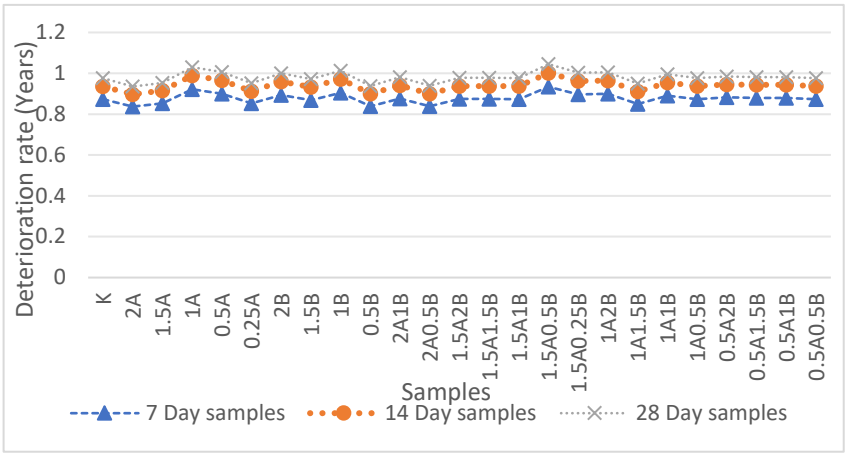


**Fig. 9 - Derived deterioration rate of the samples**
***Image by the author of the article***

On the other hand, based on Figure 10, the direct comparison among the different concrete mixes with respect to fatigue life (N) shows that mix 2A1B has a far superior fatigue performance to the other samples, likely due to its specific composition matching the optimal 0.3% basalt fiber content. As shown graphically, mix design plays a crucial role, wherein the huge variation in the derived values of N shows that not all fiber-reinforced combinations are created equal. Further, by plotting data points, it would show vividly how steep the logarithmic relation of the S-N model is, indicating that for a small reduction in applied stress level, the number of cycles to failure for each mix is exponentially increased. These results also align with Qin et al. (2024) [55] study, which indicated that fiber type, volume fraction, length, orientation, mixing/dispersion, and specimen size all change fatigue response. Some mixes with higher nominal fiber volume perform worse if fibers agglomerate or orient poorly.

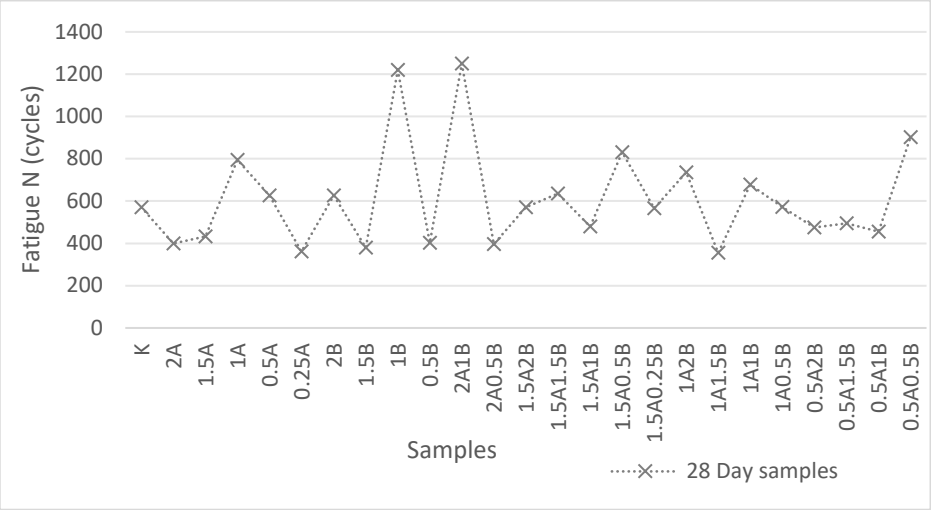


**Fig. 10 - Derived N values for 28-day pavement samples**
***Image by the author of the article***

### 3.4 Statistical Analysis Results

The Derived $\lambda_i$ values show that the 2A1B sample possessed the least expected cracks. Moreover, the results show that samples with hybrid fibers possessing higher microfiber ratios would result in lower expected cracks, i.e., 2A1B,1.5A1.5B, both of which possessed lower expected cracks than 1.5A2B (see Figure 11). In addition, lower expected cracks resulted in resistance against cracking, as shown in Figure 12. 2A1B possessed the highest $\beta$ value, thus indicating that the use of smaller fibers in fiber reinforced does improve cracking resistance of fiber-reinforced concrete more than the use of macro fiber-reinforced concrete. These results also align with He et al. (2022) [56], which indicated the importance of proper fiber hybridization ratios to increase crack bridging capacity to reduce early cracks, hence improving the crack resistance of concrete.

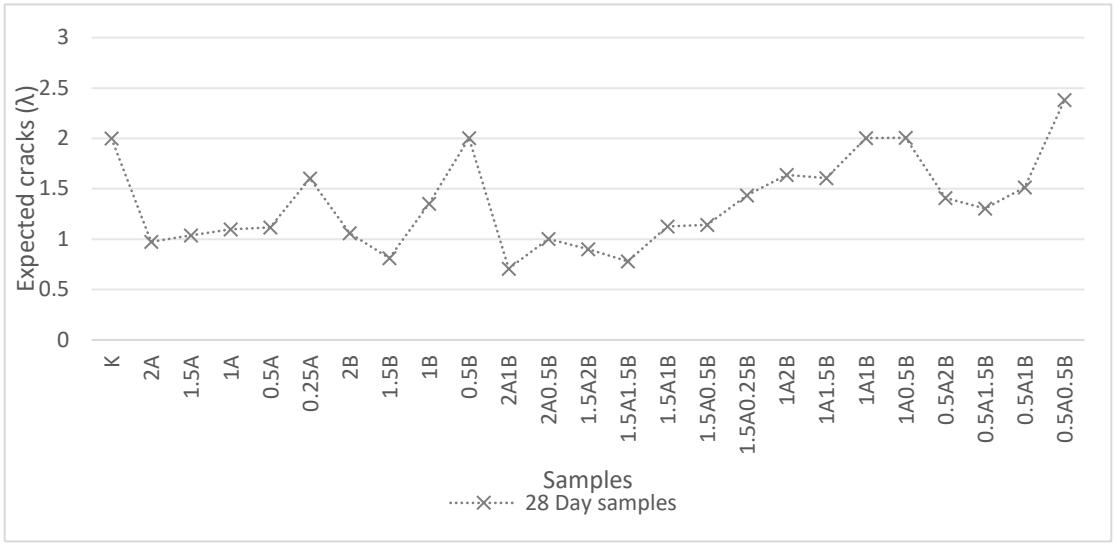


**Fig. 11 - Derived λ for 28-day pavement samples**
***Image by the author of the article***

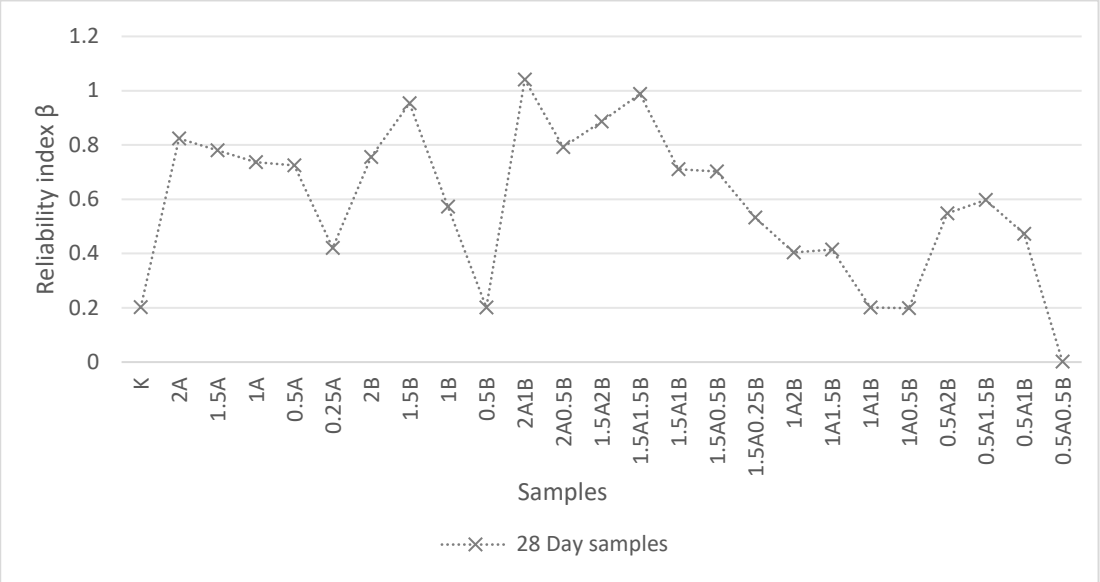


**Fig. 12 - Derived β for 28-day pavement samples**
***Image by the author of the article***

## 4 Conclusions

The present study investigated the influence of basalt fibers and different fiber combinations on the performance of concrete to be used in airport pavements. With laboratory tests, modeling tools, and reliability analysis, the investigation also explored the effects of fiber type, dosage, and hybridization on the overall behavior of pavements. The Conclusion of the study is as follows:

1. The test results showed that basalt fibers significantly enhanced performance. Greater fiber content lowered crack width and depth. Hybrid mixes worked best in limiting crack formation and slowing crack growth. Mix 1.5A0.5B showed the best fracture resistance among all mixes, evidencing more toughness and energy absorption.
2. Durability tests highlighted the importance of fiber dispersion: mix 1.5A0.5B achieved the least chloride penetration and the longest estimated service life
3. The fatigue modeling showed that performance depends on a balanced mix of fibers, rather than just the total volume. The best resistance against repeated loading was given for the 2A1B mix.
4. Reliability analysis confirmed that microfibers play a key role, and that mixes 2A1B and 1.5A1.5B have the lowest failure probabilities and the highest reliability.

To summarize, the results indicated that balanced hybrid basalt fiber systems provided improvements in resisting fracture, cracking, and fatigue performance, and durability under long-term exposure. The testing framework developed herein also provides a useful guideline to improve future FRC pavement designs. Well-designed hybrid basalt fiber reinforcements could lead to stronger, more durable, reliable, and sustainable airport pavements.

## 5 Fundings

The authors received no financial support for the research, authorship, and publication of this article.

## 6 Conflict of Interests

The authors declared no potential conflicts of interest concerning the research, authorship, and publication of this article.

## References

Qais, Q.A.A.; Kotlyarevskaya, A.; Okolnikova, G.
Hybrid basalt fiber aerodrome concrete performance evaluation,
2026; Construction of Unique Buildings and Structures; 121 Article No 12103. doi: 10.4123/CUBS.121.3

1. Xu, W., Zang, Z., Liu, X., Ji, Y., Xu, J., and Li, H. (2025). Research on mechanical properties and prediction methods of hybrid fiber concrete for airport pavements. *PloS one*, **20(11)**, e0331951. https://doi.org/10.1371/journal.pone.0331951
2. Liu, Q., Yi, X., Yu, B., Falchetto, A. C., and Wang, D. (2025). A review of high-performance fiber concrete for airport pavements. *Journal of Traffic and Transportation Engineering (English Edition)*, **12(4)**, 907-925. https://doi.org/10.1016/j.jtte.2024.06.005
3. Mao, J., Liang, N., Liu, X., Zhong, Z., and Zhou, C. (2023). Investigation on early-age cracking resistance of basalt-polypropylene fiber reinforced concrete in restrained ring tests. *Journal of Building Engineering*, **70**, 106155. https://doi.org/10.1016/j.jobe.2023.106155
4. Zhong, C., Xiao, Q., Fan, Z., Mao, W., Xing, S., Chen, J., Xiao, Y. and Zhou, J. (2025). Experimental investigation on flexural fatigue performance of recycled aggregate concrete hybrid with basalt-polyacrylonitrile fiber. *Scientific reports*, **15(1)**, 5855. https://doi.org/10.1038/s41598-025-89682-x
5. Mulheron, M., Kevern, J.T., and Rupnow, T.D. (2015). Laboratory fatigue and toughness evaluation of fiber-reinforced concrete. *Transportation Research Record*, **2508(1)**, 39-47. https://doi.org/10.3141/2508-0
6. Jagadeesh, P., Rangappa, S. M., and Siengchin, S. (2024). Basalt fibers: An environmentally acceptable and sustainable green material for polymer composites. *Construction and Building Materials*, **436**, 136834. https://doi.org/10.1016/j.conbuildmat.2024.136834
7. Ashteyat, A., Obaidat, A. T., Qerba'a, R., and Abdel-Jaber, M. T. (2024). Influence of basalt fiber on the rheological and mechanical properties and durability behavior of self-compacting concrete (SCC). *Fibers*, **12(7)**, 52. https://doi.org/10.3390/fib12070052
8. Hussain, M. V., and Dubey, S. (2023). Determination of optimum usage of basalt in strengthening of concrete. *International Journal for Research in Applied Science & Engineering Technology*, **11(9)**, 419–425. https://doi.org/10.22214/ijraset.2023.55671
9. Chiadighikaobi, P.C., Zakka, A.R., Camara, K., and Jean Paul, V. (2024). Effect of basalt fiber hybridization on the properties of concrete with charcoal additive. *Cogent Engineering*, **11(1)**, 2307184. https://doi.org/10.1080/23311916.2024.2307184
10. Gong, Y., Hua, Q., Wu, Z., Yu, Y., Kang, A., Chen, X., and Dong, H. (2024). Effect of basalt/steel individual and hybrid fiber on mechanical properties and microstructure of UHPC. *Materials*, **17(13)**, 3299. https://doi.org/10.3390/ma17133299
11. Hussain, L. N., Hamood, M. J., and Al-Shaarbaf, E. A. (2024). The behavior of UHPC deep beam using the hybrid combination of steel and basalt fibers. Results in Nonlinear Analysis, **7(3),** 226-243. https://www.nonlinear-analysis.com/index.php/pub/article/view/584
12. Johnson, J., Eswari, S., and Saravanan, R. (2024). Influence of hybrid basalt fiber with varied length on the mechanical properties of normal and high strength concrete. *Research On Engineering Structures And Materials*, **11(2)**, 679-696. https://doi.org/10.17515/resm2024.239me0413rs
13. Park, J.-G., Seo, D.-J., and Heo, G.-H. (2022). Impact resistanceand flexural performance properties of hybrid fiber-rein-forced cement mortar containing steel and carbonfibers. *Applied Sciences*, **12(19)**, 9439. https://doi.org/10.3390/app12199439
14. Barbhuiya, S., Das, B. B., and Kanavaris, F. (2024). A review of fracture propagation in concrete: Fundamentals, experimental techniques, modelling and applications. *Magazine of Concrete Research*, **76(10)**, 482-514. https://doi.org/10.1680/jmacr.23.00143
15. Le, G. K., Nguyen, H. Q., and Nguyen, T. D. (2024). Phase Field Modeling of Crack Propagation in Concrete Composite with Imperfect Interface. *Engineering, Technology & Applied Science Research*, **14(4)**, 15268-15273. https://doi.org/10.48084/etasr.7881
16. Baktheer, A., Martínez-Pañeda, E., and Aldakheel, F. (2024). Phase field cohesive zone modeling for fatigue crack propagation in quasi-brittle materials. *Computer Methods in Applied Mechanics and Engineering*, **422**, 116834. https://doi.org/10.1016/j.cma.2024.116834
17. Alrayes, O., Könke, C., Ooi, E. T., and Hamdia, K. M. (2023). Modeling cyclic crack propagation in concrete using the scaled boundary finite element method coupled with the cumulative damage-plasticity constitutive law. *Materials*, **16(2),** 863. https://doi.org/10.3390/ma16020863
18. Zhang, Y., Zhong, H., Li, D., Li, C., Wang, H., Li, Z., and Dong, W. (2024). Experimental and numerical research on fracture properties of mass concrete under quasi-static and dynamic loading. *Buildings*, **14(10)**, 3312. https://doi.org/10.3390/buildings14103312
19. Tao, J., Jing, M., Yang, Q., and Liang, F. (2025). Fracture Behaviour of Basalt Fiber-Reinforced Lightweight Geopolymer Concrete: A Multidimensional Analysis. *Materials*, **18(15)**, 3549. https://doi.org/10.3390/ma18153549

20. Ding, L., Lin, Z., Xu, C., Xu, H., Li, B., and Shen, J. (2025). Study on the hybrid effect of basalt and polypropylene fibers on the mechanical properties of concrete. *Buildings*, **15(17)**, 3197. https://doi.org/10.3390/buildings15173197
21. Khan, M., Cao, M., Xie, C., and Ali, M. (2021). Efficiency of basalt fiber length and content on mechanical and microstructural properties of hybrid fiber concrete. *Fatigue & Fracture of Engineering Materials & Structures*, **44(8)**, 2135-2152. https://doi.org/10.1111/ffe.13483
22. Zhang, J., Leung, C. K. Y., and Gao, Y. (2024). Simulation of tensile performance of fiber-reinforced cementitious composite with fracture mechanics model. *In B. H. Oh et al. (Eds.), High Performance, Fiber Reinforced Concrete, Special Loadings and Structural Applications.* https://framcos.org/FraMCoS-7/12-04.pdf
23. da Silva Neto, J. T., Ribeiro Soares Junior, P. R., Reis, E. D., de Souza Maciel, P., Gomes, P. C. C., Gouveia, A. M. C., and da Silva Bezerra, A. C. (2025). Fiber-reinforced cementitious composites: recent advances and future perspectives on key properties for high-performance design. *Discover Civil Engineering*, **2(1)**, 1-20. https://doi.org/10.1007/s44290-025-00209-9
24. Fu, Q., Zhang, Z., Xu, W., Zhao, X., Zhang, L., Wang, Y., and Niu, D. (2022). Flexural behavior and prediction model of basalt fiber/polypropylene fiber-reinforced concrete. *International Journal of Concrete Structures and Materials*, **16(1)**, 31. https://doi.org/10.1186/s40069-022-00524-w
25. Zhang, M., Chen, J., Liu, J., Yin, H., Ma, Y., and Yang, F. (2025). Fracture Behavior of Steel-fiber-Reinforced High-Strength Self-Compacting Concrete: A Digital Image Correlation Analysis. *Materials*, **18(15)**, 3631. https://doi.org/10.3390/ma18153631
26. Pei, G., Xiao, D., Zhang, M., Jiang, J., Xie, J., Li, X., and Guo, J. (2024). Study on the Dynamic Fracture Properties of Defective Basalt Fiber Concrete Materials Under a Freeze–Thaw Environment. *Materials*, **17(24)**, 6275. https://doi.org/10.3390/ma17246275
27. Tao, J., Jing, M., Yang, Q., and Liang, F. (2025). Fracture Behaviour of Basalt Fiber-Reinforced Lightweight Geopolymer Concrete: A Multidimensional Analysis. *Materials*, **18(15)**, 3549. https://doi.org/10.3390/ma18153549
28. Saouma, V. E. (2022). Notes in Fracture Mechanics. *University of Colorado*. https://civil.colorado.edu/~saouma/files/Fracture-Mechanics-Saouma.pdf.
29. Zhu, H., Huo, Q., Fan, J., Pang, S., Chen, H., and Yi, C. (2020). The depth–width correlation for shrinkage-induced cracks and its influence on chloride diffusion into concrete. *Materials*, **13(12)**, 2751. https://doi.org/10.3390/ma13122751
30. Ren, Y., Shi, J., Zhou, L., and Peng, S. (2024). Experimental study on flexural fatigue resistance of fiber-reinforced sustainable walnut shell ash mortar. *Discover Applied Sciences*, **6(11)**, 600. https://doi.org/10.1007/s42452-024-06334-x
31. Zhang, X., Lou, C., and Lyu, X. (2024). Experimental study on direct tensile fatigue performance of basalt fiber reinforced concrete. *Scientific Reports*, **14(1)**, 765. https://doi.org/10.1038/s41598-024-51403-1
32. Zhang, L. (2024). A new fatigue cumulative damage model based on material parameters and stress interaction. *International Journal of Fatigue*, **179**, 108035. https://doi.org/10.1016/j.ijfatigue.2023.108035
33. Basnet, K. S., Shrestha, J. K., and Shrestha, R. N. (2023). Pavement performance model for road maintenance and repair planning: A review of predictive techniques. *Digital Transportation and Safety*, **2(4)**, 253-267. https://doi.org/10.48130/DTS-2023-0021
34. Qin, C., Dong, X., Wu, B., Cai, L., Wang, S., and Xia, Q. (2024). Fatigue damage analysis of plain and steel fiber-reinforced concrete material based on a stiffness degradation microplane model. *Frontiers in Materials*, **11**, 1505295. https://doi.org/10.3389/fmats.2024.1505295
35. Singh, S. P., Singh, A. P., and Bajaj, V. (2012). Flexural fatigue strength of hybrid fibrous concrete beams. *Proceedings of the Institution of Civil Engineers-Construction Materials*, **165(2)**, 99-110. https://doi.org/10.1680/coma.10.0009
36. Al-Rousan, E. T., Khalid, H. R., and Rahman, M. K. (2023). Fresh, mechanical, and durability properties of basalt fiber-reinforced concrete (BFRC): A review. *Developments in the Built Environment*, **14**, 100155. https://doi.org/10.1016/j.dibe.2023.100155
37. Zhao, R., Shi, C., Zhang, R., Wang, W., Zhu, H., and Luo, J. (2024). Study on the freeze-thaw resistance of concrete pavements in seasonally frozen regions. *Materials*, **17(8)**, 1902. https://doi.org/10.3390/ma17081902

38. Guo, R., Li, J., and Huo, X. Durability Experimental Study and Service Life Evaluation of Basalt-Pva fiber-Reinforced Concrete in Chloride-Rich Environments. *Case Studies in Construction Materials*, **23**, e05060. https://doi.org/10.1016/j.cscm.2025.e05060
39. Zhou, J., Wang, G., and Zhu, G. (2023). The durability of basalt-fiber-reinforced cement mortar under exposure to unilateral salt freezing cycles. *Frontiers in Materials*, **10**, 1202889. https://doi.org/10.3389/fmats.2023.1202889
40. Wang, Z., Niu, F., Du, W., and Wang, Y. (2025). Durability evaluation of modified basalt fiber reinforced concrete in high altitude cold regions: based on AE, DIC and deep learning prediction. *Case Studies in Construction Materials*, **22**, e04837. https://doi.org/10.1016/j.cscm.2025.e04837
41. Görander, N., and Halldén, C. (2015). Crack Width Profiles for fiber-reinforced Concrete Elements with Conventional Reinforcement. https://odr.chalmers.se/bitstreams/3e2b4162-9ab8-46dc-8660-e420d8661501/download
42. Van der Esch, A., Wolfs, R., Fennis, S., Roosen, M., and Wijte, S. (2024). Categorization of formulas for calculation of crack width and spacing in reinforced concrete elements. *Structural Concrete*, **25(1)**, 32-48. https://doi.org/10.1002/suco.202300535
43. Vandewalle, L. (2003). Test and design methods for steel fiber reinforced concrete. In PRO 31: International RILEM Workshop on Test and Design Methods for Steel fiber Reinforced Concrete-Background and Experiences (Vol. 31, p. 1). RILEM Publications. https://books.google.com.ng/books?id=lMTIIQb-MO8C&lpg=PA1&dq=44.Vandewalle%2C%20L.%20(2003).%20Test%20and%20design%20methods%20for%20steel%20fiber%20reinforced%20concrete.%20In%C2%A0PRO%2031%3A%20International%20RILEM%20Workshop%20on%20Test%20and%20Design%20Methods%20for%20Steel%20fiber%20Reinforced%20Concrete-Background%20and%20Experiences%C2%A0(Vol.%2031%2C%20p.%201).%20RILEM%20Publications.&lr&pg=PP1#v=onepage&q&f=false
44. Ojha, P. N., Singh, P., Singh, B., Singh, A., and Mittal, P. (2022). Fracture behavior of plain and fiber-reinforced high strength concrete containing high strength steel fiber. *Research on Engineering Structures and Materials*, **8(3),** 583-602. https://doi.org/10.17515/resm2022.377ma1228
45. Al Fuhaid, A. F., and Alanazi, H. (2023). Prediction of chloride diffusion coefficient in concrete modified with supplementary cementitious materials using machine learning algorithms. *Materials*, **16(3)**, 1277. https://doi.org/10.3390/ma16031277
46. Xu, Q., Liu, B., Dai, L., Yao, M., and Pang, X. (2024). Factors influencing chloride ion diffusion in reinforced concrete structures. *Materials*, **17(13)**, 3296. https://doi.org/10.3390/ma17133296
47. Xu, Z., and Ye, G. (2023). Understanding chloride diffusion coefficient in cementitious materials. *Materials*, **16(9),** 3464. https://doi.org/10.3390/ma16093464
48. Chen, H., Sun, Z., Zhang, X., and Fan, J. (2023). Tensile fatigue properties of ordinary plain concrete and reinforced concrete under flexural loading. *Materials*, **16(19)**, 6447. https://doi.org/10.3390/ma16196447
49. Ren, Y., Shi, J., Zhou, L., and Peng, S. (2024). Experimental study on flexural fatigue resistance of fiber-reinforced sustainable walnut shell ash mortar. *Discover Applied Sciences*, **6(11)**, 600. https://doi.org/10.1007/s42452-024-06334-x
50. Szép, J., Habashneh, M., Lógó, J., and Movahedi Rad, M. (2023). Reliability assessment of reinforced concrete beams under elevated temperatures: a probabilistic approach using finite element and physical models. *Sustainability*, **15(7)**, 6077. https://doi.org/10.3390/su15076077
51. Xue, Z., Qi, P., Yan, Z., Pei, Q., Zhong, J., and Zhan, Q. (2023). Mechanical properties and crack resistance of basalt fiber self-compacting high strength concrete: an experimental study. *Materials*, **16(12)**, 4374. https://doi.org/10.3390/ma16124374
52. Anas, M., Khan, M., Bilal, H., Jadoon, S., and Khan, M. N. (2022). fiber reinforced concrete: a review. *Engineering Proceedings*, **22(1)**, 3. https://doi.org/10.3390/engproc2022022003
53. Chiadighikaobi, P. C., Muritala, A. A., Mahadi, M. I. A., Abd Noor, A. A., Ibitogbe, E. M., and Niazmand, A. M. (2022). Mechanical characteristics of hardened basalt fiber expanded clay concrete cylinders. *Case Studies in Construction Materials*, **17**, e01368. https://doi.org/10.1016/j.cscm.2022.e01368
54. Razmi, A., Bennett, T., Xie, T., and Visintin, P. (2025). A phenomenological model for chloride diffusion coefficient in concretes with traditional and blended binders and alternative

fillers. *Construction and Building Materials*, **461**, 139783. https://doi.org/10.1016/j.conbuildmat.2024.139783

55. Qin, C., Dong, X., Wu, B., Cai, L., Wang, S., and Xia, Q. (2024). Fatigue damage analysis of plain and steel fiber-reinforced concrete material based on a stiffness degradation microplane model. *Frontiers in Materials*, **11**, 1505295. https://doi.org/10.3389/fmats.2024.1505295
56. He, F., Biolzi, L., and Carvelli, V. (2022). Effect of fiber hybridization on mechanical properties of concrete. *Materials and Structures*, **55(7)**, 195. https://doi.org/10.1617/s11527-022-02020-9